Clinical Ophthalmology

Dovepress
open access to scientific and medical research

Open Access Full Text Article

ORIGINAL RESEARCH

Machine Learning Analysis Classifies Patients with Primary Angle-Closure Glaucoma Using Abnormal Brain White Matter Function

Qiu-Yu Tang[1,*], Yu-Lin Zhong[2,*], Xin-Miao Wang[3,*], Bing-Lin Huang[1], Wei-Guo Qin[4], Xin Huang[2]

[1]College of Clinical Medicine, Jiangxi University of Chinese Medicine, Nanchang City, Jiangxi, 330004, People's Republic of China; [2]Department of Ophthalmology, Jiangxi Provincial People's Hospital, The First Affiliated Hospital of Nanchang Medical College, Nanchang, Jiangxi, 330006, People's Republic of China; [3]School of Ophthalmology and Optometry, Jiangxi Medical College, Nanchang University, Nanchang, Jiangxi, 330000, People's Republic of China; [4]Department of Cardiothoracic Surgery, The 908th Hospital of Chinese People's Liberation Army Joint Logistic Support Force', Nanchang, People's Republic of China

*These authors contributed equally to this work

Correspondence: Xin Huang, Department of ophthalmology, Jiangxi Provincial People's Hospital, No. 152, Ai Guo Road, Dong Hu District, Nanchang, Jiangxi, 330006, People's Republic of China, Tel +86 15879215294, Email 334966891@qq.com

Objective: Primary angle-closure glaucoma (PACG) is a globally prevalent, irreversible eye disease leading to blindness. Previous neuroimaging studies demonstrated that PACG patients were associated with gray matter function changes. However, whether the white matter(WM) function changes in PACG patients remains unknown. The purpose of the study is to investigate WM function changes in the PACG patients.

Methods: In total, 40 PACG patients and 40 well-matched HCs participated in our study and underwent resting-state functional magnetic resonance imaging (rs-fMRI) scans. We compared between-group differences between PACG patients and HC in the WM function using amplitude of low-frequency fluctuations (ALFF). In addition, the SVM method was applied to the construction of the PACG classification model.

Results: Compared with the HC group, ALFF was attenuated in right posterior thalamic radiation (include optic radiation), splenium of corpus callosum, and left tapetum in the PACG group, the results are statistically significant (GRF correction, voxel-level $P < 0.001$, cluster-level $P < 0.05$). Furthermore, the SVM classification had an accuracy of 80.0% and an area under the curve (AUC) of 0.86 for distinguishing patients with PACG from HC.

Conclusion: The findings of our study uncover abnormal WM functional alterations in PACG patients and mainly involves vision-related regions. These findings provide new insights into widespread brain damage in PACG from an alternative WM functional perspective.

Keywords: primary angle-closure glaucoma, amplitude of low frequency fluctuations, white matter, support vector machine

Introduction

Glaucoma represents the leading cause of irreversible blindness worldwide, predominantly affecting middle-aged and elderly individuals and significantly diminishing the quality of life for patients. Currently, it afflicts over 70 million individuals globally, with projections indicating an anticipated increase to 112 million by 2040, thereby establishing itself as a major public health concern on a global scale.[1–3] As the observation and research on glaucoma continue to deepen, it has been recognised that glaucoma is mainly characterised by progressive loss of retinal ganglion cells (RGC) and their axons, enlargement of the optic disc cupping and visual field defects.[4–6] Glaucoma is broadly categorized into primary open-angle glaucoma (POAG) and primary angle-closure glaucoma (PACG) due to their distinct pathogenic mechanisms. Notably, in Asian countries, PACG is more prevalent than POAG.[7–9] PACG leads to more extensive RGC damage due to anatomical eye abnormalities, such as shallow central anterior chamber depth, atrial angle closure, obstructed aqueous

Received: 26 November 2023
Accepted: 5 February 2024
Published: 7 March 2024

drainage, and increased intraocular pressure (IOP).[10,11] The findings from previous animal experiments[12] and human autopsy studies[13] have demonstrated that glaucoma affects various structures, including the retrobulbar optic nerve, lateral geniculate body, and visual cortex, in addition to the retina. This indicates that glaucoma is not solely an ocular condition but also a form of central neurodegenerative disease that impacts the entire visual pathway and visual cortex.

Functional magnetic resonance imaging (fMRI) is an imaging method that can reflect the functional state of tissues or organs, and has been widely used in clinical and basic research on brain function. fMRI is a kind of imaging means that combines anatomy, function, and imaging, and it can correspond the damaged local brain tissues with the missing function corresponds to the damaged local brain tissue and the missing function, and is now widely used in the study of histomorphology and pathological mechanisms of neurological central nervous system diseases.[14] Resting-state functional magnetic resonance imaging (rs-fMRI) can reveal the spontaneous neuronal activity of the brain during rest, enabling the observation of functional changes in the brain WM non-invasively. It is widely utilized for studying neurodegenerative diseases.[15,16] In recent years, researchers have utilized rs-fMRI based on blood oxygen level-dependent (BOLD) signals to identify neuronal activity in the grey matter (GM) of the cerebral cortex, while disregarding signals from the white matter (WM) due to the prior assumption that there are few postsynaptic potentials in the WM resulting in weak BOLD signals.[17,18] Therefore, previous studies have primarily focused on investigating structural changes in the WM tissue of glaucoma patients. The prominence of cerebral WM loss in the central visual pathway of patients may indicate the severity of glaucoma.[19,20] However, there is accumulating evidence suggesting that the vasculature and perfusion of the WM are capable of accommodating hemodynamic changes that can be detected by BOLD fMRI.[21–24] This has the potential to revolutionize the study of WM in both healthy and diseased individuals. Gawryluk et al[25] utilizing a 4T fMRI approach, observed neural activity activation in WM regions when stimulated by gustatory, motor, and visual tasks. They noted that the degree of activation varied depending on the type of task. Brandt et al[26] employed fMRI to administer coherent motor stimulation to the left and right hemivision cortex in normal subjects. Their findings revealed a negative signal change in the contralateral optic radiation bundle of the visually stimulated hemisphere within the occipital lobe of the brain's WM. Peer et al[27] utilized Fourier transforms to determine that the resting-state WM functional network exhibits a strong correlation with the GM functional network. Their findings suggest that identifying the WM could provide valuable insights to enhance our comprehension of the GM functional network. This discovery could potentially lead to new directions for research in cognitive neuroscience and clinical neuropsychiatry. When considered collectively, these studies provide compelling evidence for the presence of meaningful signals in WM and affirm the efficacy of BOLD fMRI in detecting low-frequency fluctuations in WM. Despite this, there is a notable absence of research investigating abnormal functional changes in the WM of patients with PACG.

Amplitude of low-frequency fluctuations (ALFF) is the most widely used analytical technique in rs-fMRI and is capable of revealing localized neural activity of the brain in the resting state, with high sensitivity to potential alterations in brain function. The ALFF serves as a representative measure of brain functional activity across diverse physiological states, and it is characterized by high reliability and reproducibility.[28] In previous investigations, researchers[29–31] have documented spontaneous neural activity in the GM of individuals affected by PACG. Their findings indicated a reduction in ALFF in regions encompassing the visual cortex, sensorimotor cortex, frontal lobe, frontoparietal network, and default mode network among PACG patients. These observations suggest a link between abnormal functioning in the central nervous system and impaired visual, cognitive, and emotional capabilities in individuals with PACG. It is noteworthy that individuals with glaucoma are at an elevated risk of developing cognitive decline disorders, including AD and PD.[32–35] According to prior research,[36–39] the application of ALFF has been utilized to investigate the abnormal WM function in diverse neurological conditions, including AD, PD, and Schizophrenia. Based on this background, we applied the ALFF brain functional index to explore WM functional changes in patients with PACG.

Machine learning algorithms are commonly employed in neuroimaging data analysis to reveal disease-associated insights, develop personalized predictive models, and differentiate between patients and HCs.[40–42] Support vector machine (SVM) is among the most extensively employed machine learning methods for MRI classification, facilitating highly accurate disease classification and assessment at the individual level.[43] SVM is able to handle high dimensional data efficiently, provide better classification performance, show strong performance in small sample scenarios, and help to build reliable classifiers in limited data situations. In previous studies, SVM have been integrated with rs-fMRI to

achieve optimal predictive results for lesion classification by identifying patients and HCs based on abnormal signal values.[44–48] Therefore, we applied the SVM approach to test whether abnormal WM function can effectively differentiate PACG patients from HCs.

This study utilized the resting-state indicator ALFF to investigate functional alterations in the WM in patients with PACG, aiming to ascertain the presence of functional impairments in the WM of PACG patients. Additionally, the SVM algorithm was employed to evaluate whether the altered WM function of ALFF could serve as a distinguishing feature for identifying PACG patients from HCs.

Methods

Participants

We selected PACG patients attending the Department of Ophthalmology of Jiangxi Provincial People's Hospital as the study population. Healthy volunteers matched for gender and age were recruited as healthy controls during the same time period. In this study, a total of 40 patients diagnosed with PACG in both eyes and 40 healthy controls, matched for gender and age, were included. The inclusion criteria for the PACG patient cohort were as follows: (1) Intraocular pressure exceeding 21 mmHg; (2) Presence of closed-angle glaucoma signs, such as a shallow anterior chamber and narrowing of the angle of the anterior chamber; (3) Optic disc alteration with a cup-to-disc ratio (C/D) greater than 0.6 as observed through fundus examination; (4) Presence of distinctive glaucomatous visual field defects, such as a dark spot in the paracentral area, a bow-shaped dark spot, a nasal stepped visual field defect, a fan-shaped visual field defect, a tubular visual field, etc.; (5) Absence of any other ocular diseases; (6) No contraindications for magnetic resonance examination.

Exclusion criteria for all subjects were (1) open-angle glaucoma, normal intraocular pressure glaucoma, high myopia, and strabismus; (2) those with psychiatric disorders and a history of traumatic brain injury (3) those with a history of alcohol and drug abuse; (4) those who were claustrophobic or who could not adapt to the environment of the magnetic resonance scanning; and (5) those with incomplete clinical data.

Statement of Ethics

The study was carried out in accordance with the principles set forth in the Declaration of Helsinki and received approval from the ethical committee of Jiangxi Provincial People's Hospital. Before participation, all individuals involved in the study provided written informed consent.

MRI Acquisition

The data acquisition took place in the magnetic resonance examination room at Jiangxi Provincial People's Hospital, using a 3.0T magnetic resonance scanner (Discovery MR 750W system; GE Healthcare, Milwaukee, WI, USA). Subjects were positioned in a supine posture, with earplugs to reduce scanning noise, and their heads were secured with sponge pads for whole-brain scanning. (1) Whole-brain T1 images were obtained with three-dimensional brain volume imaging (3D-BRAVO) MRI with the following parameters: repetition time = 8.5 ms, echo time = 3.3 ms, thickness=1.0 mm, no layer spacing, acquisition matrix=256×256, field of view=240×240 mm^2, and flip angle=12°. (2)Functional images were obtained by using a gradientecho-planar imaging sequence with the following parameters: repetition time= 2000.0 ms, echo time= 25.0 ms, thickness= 3.0 mm, layer spacing= 1.2 mm, matrix 64 × 64, field of view= 240 mm × 240 mm^2, flip angle=12°, voxel size =3.6×3.6×3.6 mm^3, and 35 axial slices. During the scanning process, subjects were instructed to close their eyes, remain motionless, and breathe calmly while staying awake.

Rs-fMRI Data Preprocessing

The data underwent sorting and identification of incomplete or defective data, which were then excluded using MRIcro software. Image preprocessing was conducted using the Data Processing and Analysis for (Resting-State) Brain Imaging (DPABI) software, including the following steps: (1) Removal of the first 10 time points to stabilize magnetization intensity, and correction of raw images for slice time and head motion. (2) Segmentation of the T1 image into WM, GM, and cerebrospinal fluid (CSF), and alignment with the mean BOLD image generated during motion correction. (3)

Removal of linear trends to correct for signal drift. (4) Noise signal regression. To avoid eliminating signals of interest, we regressed only head movements and CSF means, without regressing WM and whole-brain signals were excluded. (5) We extracted individual-level WM 4D images by defining each voxel as GM, WM, and CSF based on the maximum probability in the T1 image segmentation results. (6)Spatial smoothing (FWHM=4mm) was performed on the WM and GM images of each subject, respectively. (7) Creation of grouplevel WM masks based on individual-level WM 4D images for follow-up statistical analysis. Voxels identified as WM in >90% of participants were adopted to create the WM mask. The subcortical regions were then removed from the WM mask based on the Harvard–Oxford Atlas. The WM mask was also coregistered to the functional space and resampled to process the functional image.

ALFF of WM Calculation

The ALFF was calculated using the DPABI Data Analysis Toolkit. The power spectrum was derived by transforming the smoothed signal of each voxel from the time series to the frequency domain using the fast Fourier transform (FFT). Subsequently, the square root of each power spectrum frequency was calculated in the 0.01 ~ 0.15 Hz band, yielding the average square root of each voxel. Finally, the ALFF value for each voxel was divided by the average ALFF value.

Support Vector Machine Analysis

The SVM algorithm was executed using the Pattern Recognition for Neuroimaging Toolbox (PRoNTo) software developed at the Cyclotron Research Centre, University of Liège, Belgium.[49] The process involved the following steps: (1) dataset specification, (2) using the mean ALFF values of WM regions with significant differences between the two groups as a classification feature, (3) applying the leave-one-out cross-validation (LOOCV) technique to validate the SVM classifier for model estimation. Within each LOOCV fold, FC data from n-1 samples were chosen as the training dataset to train the classification model. (4) Calculations were performed to determine the total accuracy, specificity, sensitivity, and area under the receiver operating characteristic curve (AUC).

Statistical Analysis

The clinical characteristics of the two groups were statistically analyzed using the Statistical Package for Social Sciences (SPSS) 26 by IBM Corp., Armonk, N.Y., USA. Gender comparisons were conducted using the chi-square test, while age, education, best-corrected visual acuity (BCVA) and IOP were compared using the two-sample *t*-test. Differences in WM ALFF values between the PACG and HC groups were regressed at the group level with two-sample t-tests and age, sex, and head movement as covariates by the Data Analysis Module on the DPABI Toolkit (http://rfmri.org/DPABI). Multiple comparisons were corrected using the Gaussian Random Field (GRF) method, with a voxel-level significance set at $P < 0.001$ (two-tailed) and cluster-level significance set at $P < 0.05$. Brain regions demonstrating differences between groups in the metric analysis were identified based on the ICBM-DTI-81 white-matter label atlas (JHU DTI-based WM atlases, provided by Dr. Susumu Mori, Laboratory of Brain Anatomical MRI, Johns Hopkins University)[50,51] A schematic of the analysis is presented in Figure 1.

Results

Demographics and Visual Measurements Between Two Groups

The independent sample *t*-test was used to investigate the clinical features between the two groups, there was no statistically significant difference ($P>0.05$). But the differences in in BAVC and IOP was statistically significant in the right eye ($P<0.001$) and left eye ($P<0.001$). Specific information is detailed in Table 1.

Different ALFF Values Between Two Groups

The disparities in WM ALFF signal values between the PACG and HC groups were examined, and the average distribution of WM ALFF signal values between the PACG and HC groups is depicted in Figure 2.

The results reveal a statistically significant attenuation of ALFF in the Posterior thalamic radiation (including the optic radiation) R, Splenium of corpus callosum, and Tapetum_L in the PACG group compared to the HC group (corrected for GRF, voxel-level $P < 0.001$, cluster-level $P < 0.05$; see Figure 3 and Table 2).

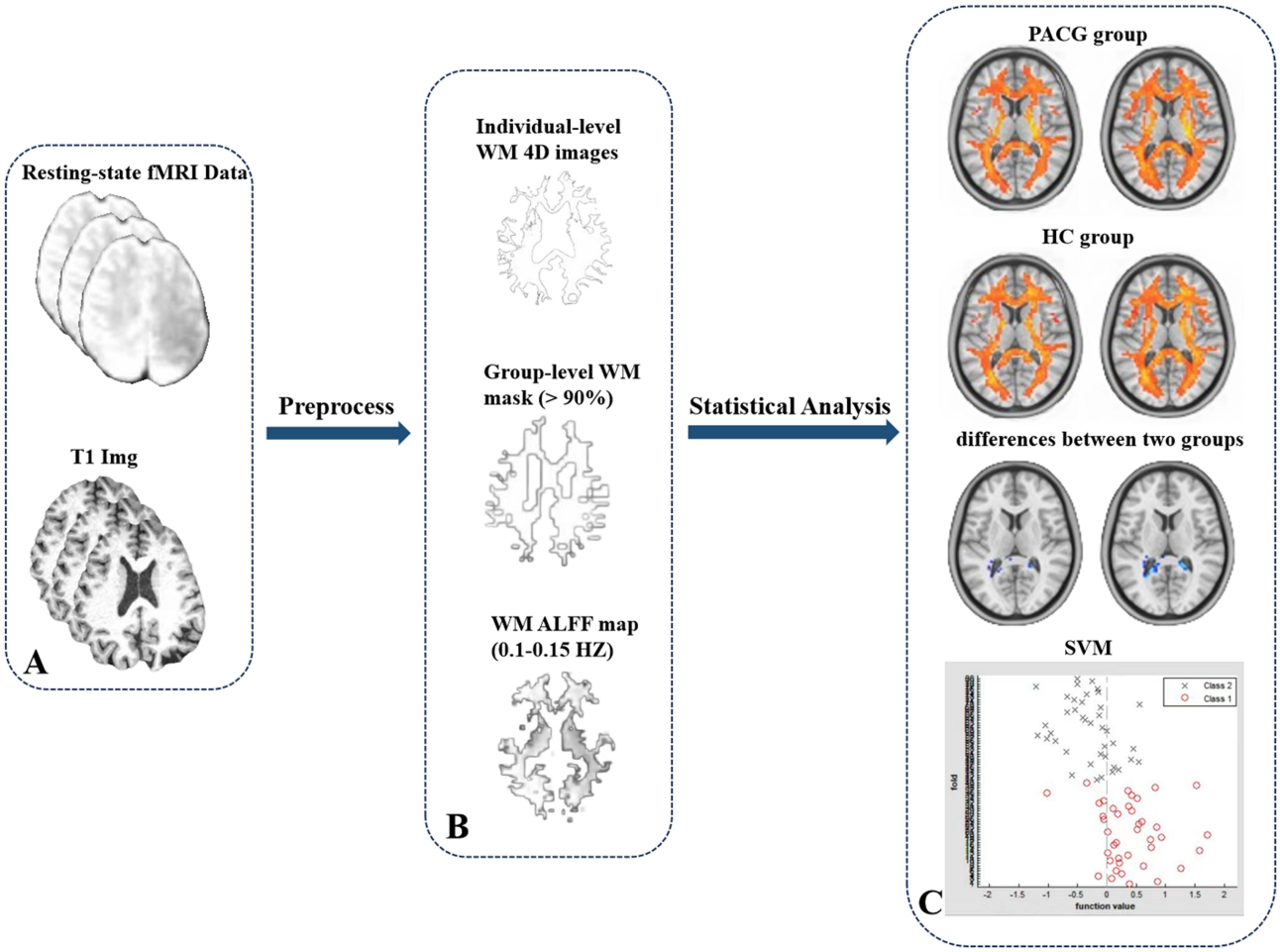

Figure 1 Flow chart of preprocessing, metric calculation, and statistical analysis in this study. Data acquisition of fMRI and T1 in subjects (**A**) white matter function calculation(**B**) Differences in white matter function between the two groups and machine learning (**C**).

Support Vector Machine Results

The machine learning analysis yielded classification results along with the ROC curve of the classifier, depicted in Figure 4. The SVM classification achieved an overall accuracy of 80.0%. The classification was based on ALFF values,

Table 1 Demographics and Visual Measurements Between Two Groups

Condition	PACG Group	HC Group	T-Value	P-value
Gender (male/female)	23/17	19/21	N/A	0.370
Age (years)	57.31 ± 11.60	55.36 ± 13.52	0.692	0.491
BCVA-OD	0.38 ± 0.52	1.13 ± 0.16	−8.718	< 0.001*
BCVA-OS	0.43 ± 0.37	1.07 ± 0.25	−9.064	< 0.001*
IOP-L(mmHg)	21.95±4.07	15.26±1.25	−9.937	< 0.001*
IOP-R(mmHg)	22.58±5.71	15.75±2.18	−7.067	< 0.001*
MD-L(dB)	−11.76±9.25	N/A	N/A	N/A
MD-R(dB)	−12.77±10.56	N/A	N/A	N/A

Notes: Chi-square test for gender; Independent *t*-test was used for other normally distributed continuous data. Data are presented as mean ± standard deviation. *p < 0.001.
Abbreviations: PACG, primary angle-closure glaucoma; HC, healthy control; BCVA, best-corrected visual acuity; OD, oculus dexter; OS, oculus sinister; IOP, Intraocular pressure; MD, Mean deviation of visual field; L, left; R, right; N/A, not applicable.

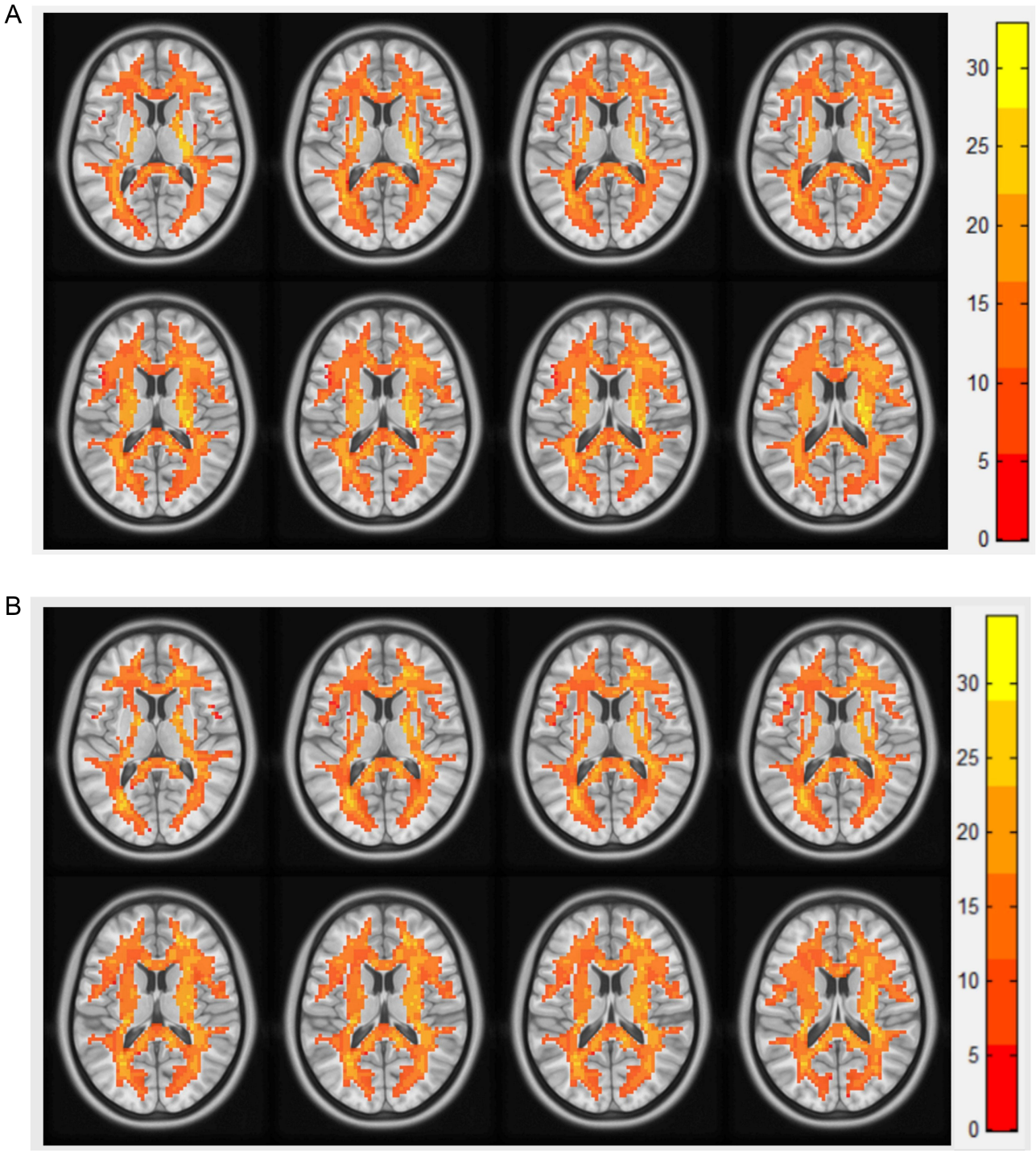

Figure 2 Results of the two components representing the white matter ALFF signal values by one-sample *t*-test in patients with (**A**) PACG and (**B**) HC.

with class 1 representing the PACG group and class 2 the HC group (Figure 4A). Additionally, the three-dimensional confusion matrices resulting from the machine learning analysis are presented in Figure 4B, while the function values of the two groups (class 1: PACG group; class 2: HC group) are illustrated in Figure 4C. Lastly, Figure 4D displays the ROC curve of the SVM classifier, demonstrating an AUC value of 0.86.

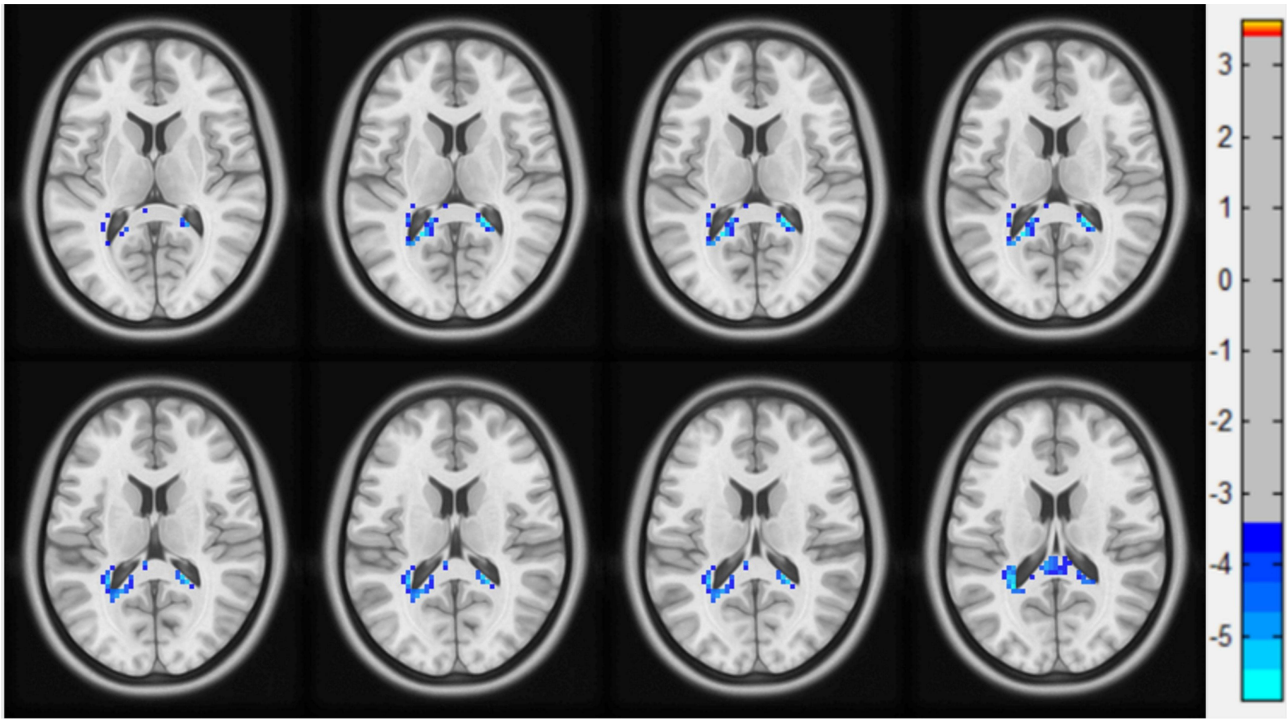

Figure 3 Regions of WM showing ALFF differences between PACG and HC groups.

Discussion

In this investigation, we employed resting-state ALFF methods to identify abnormal WM function in the brains of PACG patients. Comparative analysis with HCs revealed significantly lower ALFF values in the right Posterior thalamic radiation (including optic radiation), Splenium of corpus callosum, and left Tapetum among PACG patients. The SVM classifier achieved an overall accuracy of 80.00%, and the AUC value of the ROC curve was 0.86 (r=0.25). These observations may indicate the presence of functional impairment in the cerebral WM of PACG patients, potentially contributing to visual, memory, cognitive, and emotional challenges. Consequently, these findings may offer novel insights into functional changes in the brain WM in PACG patients.

The ALFF values for the right-sided Posterior Thalamic Radiation (PTR), which encompasses the optic radiation, were markedly lower in PACG patients than in HC. The PTR is composed of nerve fibers connecting the thalamus to the occipital lobe, including projection fibers from the thalamus to the cortex, the optic radiation from the lateral geniculate body to the visual cortex, and critical regions of the default mode network (DMN) like the posterior cingulate. These structures are primarily associated with functions involving executive control, attention, memory, and visual processing.[52–54] Injuries to the posterior thalamic radiation, encompassing the optic radiation, may result in transient or enduring visual deficits, including visual disturbances, nystagmus, and strabismus. Additionally, the patient's cognitive

Table 2 Regions of WM Showing Abnormal ALFF in Patients with PACG Compared with HCs

Metrics	Tract (JHU-Atlas)	Voxels	MNI Coordinates			T value
			x	y	z	
ALFF	Posterior thalamic radiation (include optic radiation) R	94	−33	−42	18	−3.42476
	Splenium of corpus callosum	65	−6	−36	9	−3.42013
	Tapetum_L	27	21	−42	21	−3.52558

Note: The statistical threshold was set at voxel with P <0:001 and cluster with P <0:05 for GRF correction.
Abbreviations: WM, white matter; ALFF, amplitude of low-frequency fluctuation; PACG, primary angle-closure glaucoma; HC, healthy control; MNI, Montreal Neurological Institute; x, y, and z are the locations of the peak voxels in standard MNI coordinates; R, right; L, left.

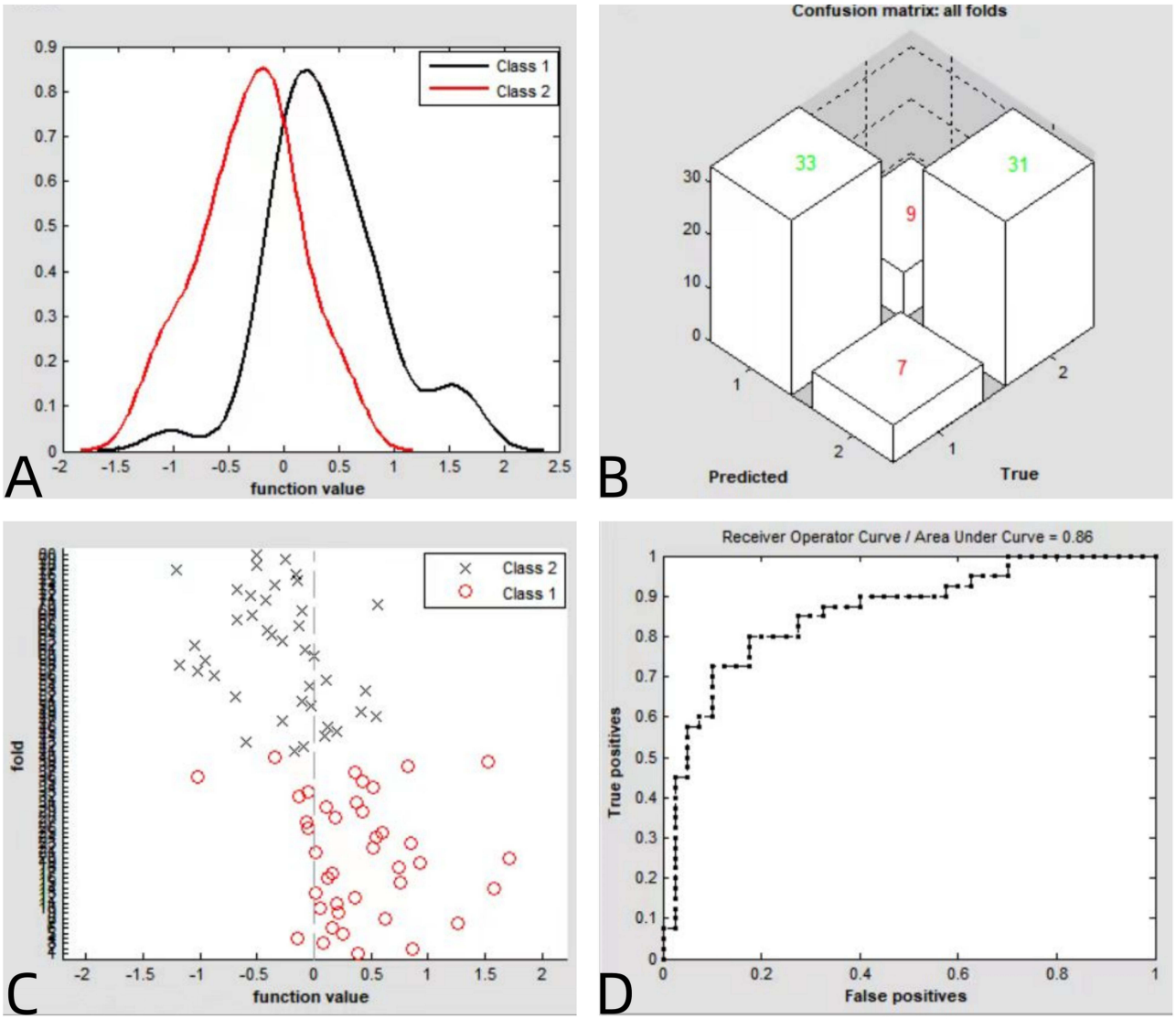

Figure 4 (**A**)Classification results using machine learning analysis based on ALFF values; (**B**)three dimensional confusion matrices from machine learning analysis; (**C**) function values of two groups with a scatter diagram; (**D**) the ROC curve of the SVM classifier with an AUC value of 0.86. (class 1: PACG group; class 2: HC group).

abilities, self-care, emotional expression, and motor functions could be impacted by the visual impairment.[55–57] Prior researches[58–60] have reported damage to cerebral WM structures associated with vision and cognition in glaucoma patients and structural alterations in the visual pathway in glaucoma patients compared to HCs. In the present study, the ALFF values of the right PTR (including optic radiation) of PACG patients were significantly decreased, suggesting that the function of the main visual pathway is impaired in PACG patients. In addition, we hypothesized that patients with glaucoma may have broader alterations in brain function related to the visual system.

The corpus callosum(CC), the brain's largest WM fiber structure, serves as a crucial pathway connecting the left and right cerebral hemispheres. It plays a significant role in facilitating information transfer and integration between the hemispheres, among other functions.[61,62] Damage to the CC is strongly linked to various cognitive declines, encompassing memory, emotion, and execution.[63] In this study, reduced ALFF was observed in the splenium of the CC and left tapetum in patients with PACG compared to HCs. The fiber bundles in the posterior section of the CC connect to the occipital cortex, aiding the occipital lobe in visual information processing, information transfer, and integration.[64,65] Previous studies[66,67] have demonstrated that infarctions affecting the CC and the corpus cavernosum can lead to diminished visuospatial and attentional capabilities to varying extents. The reduction in ALFF values observed in the

posterior section of CC during this study indicates that functional disturbances in cerebral WM among PACG patients may potentially lead to a progressive disruption of their cerebral cognitive networks, resulting in more widespread cognitive impairment. The tapetum is a thin rim of bidirectional CC fibers connecting the temporal and occipital lobes and transmits visual information from the visual cortex to the contralateral temporal lobe, and the tapetum is critical for ensuring that neurological information is transmitted and integrated between the correct hemispheres at a localized level with nearby brain regions.[68–70] Our results suggest that the tapetum ALFF values imply a disruption in the transmission and processing of visual information in patients with PACG.

This study utilized a machine learning technique, specifically SVM, to ascertain the capacity of abnormal ALFF values in distinguishing patients with PACG from HCs. The SVM classifier achieved an overall accuracy of 80.00%, and the AUC value of the ROC curve for the SVM classifier was 0.86 (r = 0.25). The results indicate that abnormal ALFF values in brain WM could serve as a potential imaging biomarker for discriminating PACG patients from HCs. Therefore, the integration of ALFF analysis and machine learning holds promise for disease classification and diagnosis, with potential applications in future clinical practice.

Limitations

However, the present study has several limitations. Firstly, the relatively small sample size may impact the generalizability of the findings, and we aim to validate our results with a larger sample size in future research. Secondly, the scanner environment can induce stress and anxiety in subjects, particularly patients, potentially affecting brain activation and consequently influencing fMRI results. Lastly, the absence of clinical staging to evaluate the severity of the PACG patients' condition may have influenced the results to a certain extent.

Conclusion

The present study shows abnormal WM functional alterations in PACG patients and mainly involves vision-related regions. These findings provide new insights into widespread brain damage in PACG from an alternative WM functional perspective. Furthermore, the observed abnormal ALFF values in brain WM could potentially serve as a neural marker for distinguishing PACG patients from HCs.

Acknowledgments

We acknowledge the assistance provided by the National Natural Science Foundation of China (82104935), the Natural Science Foundation of Jiangxi Province (20212BAB216058), Jiangxi Provincial Health Technology Project (202210012, 202310114 and 202410008), and Jiangxi Provincial traditional Chinese Technology Project (2022B840 and 2023A0138).

Disclosure

The authors report no conflicts of interest in this work.

References

1. Stein JD, Khawaja AP, Weizer JS. Glaucoma in adults-screening, diagnosis, and management: a review. *JAMA*. 2021;325(2):164–174. doi:10.1001/jama.2020.21899
2. Reis TF, Paula JS, Furtado JM. Primary glaucomas in adults: epidemiology and public health-A review. *Clin Exp Ophthalmol*. 2022;50(2):128–142. doi:10.1111/ceo.14040
3. Schuster AK, Erb C, Hoffmann EM, Dietlein T, Pfeiffer N. The diagnosis and treatment of glaucoma. *Dtsch Arztebl Int*. 2020;117(13):225–234. doi:10.3238/arztebl.2020.0225
4. Weinreb RN, Aung T, Medeiros FA. The pathophysiology and treatment of glaucoma: a review. *JAMA*. 2014;311(18):1901–1911. doi:10.1001/jama.2014.3192
5. Gossman CA, Christie J, Webster MK, Linn DM, Linn CL. Neuroprotective strategies in glaucoma. *Curr Pharm Des*. 2016;22(14):2178–2192. doi:10.2174/1381612822666160128144747
6. Artero-Castro A, Rodriguez-Jimenez FJ, Jendelova P, VanderWall KB, Meyer JS, Erceg S. Glaucoma as a neurodegenerative disease caused by intrinsic vulnerability factors. *Prog Neurobiol*. 2020;193:101817. doi:10.1016/j.pneurobio.2020.101817
7. Wang N, Wu H, Fan Z. Primary angle closure glaucoma in Chinese and Western populations. *Chin Med J*. 2002;115(11):1706–1715.
8. Yip JL, Foster PJ. Ethnic differences in primary angle-closure glaucoma. *Curr Opin Ophthalmol*. 2006;17(2):175–180. doi:10.1097/01.icu.0000193078.47616.aa

9. Cheng JW, Zong Y, Zeng YY, Wei RL, Acott TS. The prevalence of primary angle closure glaucoma in adult Asians: a systematic review and meta-analysis. *PLoS One*. 2014;9(7):e103222. doi:10.1371/journal.pone.0103222
10. George R, Panda S, Vijaya L. Blindness in glaucoma: primary open-angle glaucoma versus primary angle-closure glaucoma-a meta-analysis. *Eye*. 2022;36(11):2099–2105. doi:10.1038/s41433-021-01802-9
11. Sun X, Dai Y, Chen Y, et al. Primary angle closure glaucoma: what we know and what we don't know. *Prog Retin Eye Res*. 2017;57:26–45. doi:10.1016/j.preteyeres.2016.12.003
12. Ito Y, Shimazawa M, Chen YN, et al. Morphological changes in the visual pathway induced by experimental glaucoma in Japanese monkeys. *Exp Eye Res*. 2009;89(2):246–255. doi:10.1016/j.exer.2009.03.013
13. Gupta N, Ang LC, Noël de Tilly L, Bidaisee L, Yücel YH. Human glaucoma and neural degeneration in intracranial optic nerve, lateral geniculate nucleus, and visual cortex. *Br J Ophthalmol*. 2006;90(6):674–678. doi:10.1136/bjo.2005.086769
14. Glover GH. Overview of functional magnetic resonance imaging. *Neurosurg Clin N Am*. 2011;22(2):133–9, vii. doi:10.1016/j.nec.2010.11.001
15. Smitha KA, Akhil Raja K, Arun KM, et al. Resting state fMRI: a review on methods in resting state connectivity analysis and resting state networks. *Neuroradiol J*. 2017;30(4):305–317. doi:10.1177/1971400917697342
16. Kang L, Wan C. Application of advanced magnetic resonance imaging in glaucoma: a narrative review. *Quant Imaging Med Surg*. 2022;12(3):2106–2128. doi:10.21037/qims-21-790
17. Logothetis NK, Pauls J, Augath M, Trinath T, Oeltermann A. Neurophysiological investigation of the basis of the fMRI signal. *Nature*. 2001;412(6843):150–157. doi:10.1038/35084005
18. Logothetis NK, Parker A, Derrington A, Blakemore C. The neural basis of the blood-oxygen-level-dependent functional magnetic resonance imaging signal. *Philos Trans R Soc Lond B Biol Sci*. 2002;357(1424):1003–1037. doi:10.1098/rstb.2002.1114
19. Sidek S, Ramli N, Rahmat K, Ramli NM, Abdulrahman F, Tan LK. Glaucoma severity affects diffusion tensor imaging (DTI) parameters of the optic nerve and optic radiation. *Eur J Radiol*. 2014;83(8):1437–1441. doi:10.1016/j.ejrad.2014.05.014
20. Wang J, Zhang Y, Meng X, Liu G. Application of diffusion tensor imaging technology in glaucoma diagnosis. *Front Neurosci*. 2023;17:1125638. doi:10.3389/fnins.2023.1125638
21. Gawryluk JR, Mazerolle EL, D'Arcy RC. Does functional MRI detect activation in white matter? A review of emerging evidence, issues, and future directions. *Front Neurosci*. 2014;8:239. doi:10.3389/fnins.2014.00239
22. Li J, Biswal BB, Meng Y, et al. A neuromarker of individual general fluid intelligence from the white-matter functional connectome. *Transl Psychiatry*. 2020;10(1):147. doi:10.1038/s41398-020-0829-3
23. Fabri M, Polonara G. Functional topography of human corpus callosum: an FMRI mapping study. *Neural Plast*. 2013;2013:251308. doi:10.1155/2013/251308
24. Fabri M, Polonara G, Mascioli G, Salvolini U, Manzoni T. Topographical organization of human corpus callosum: an fMRI mapping study. *Brain Res*. 2011;1370:99–111. doi:10.1016/j.brainres.2010.11.039
25. Gawryluk JR, D'Arcy RC, Mazerolle EL, Brewer KD, Beyea SD. Functional mapping in the corpus callosum: a 4T fMRI study of white matter. *Neuroimage*. 2011;54(1):10–15. doi:10.1016/j.neuroimage.2010.07.028
26. Brandt T, Stephan T, Bense S, Yousry TA, Dieterich M. Hemifield visual motion stimulation: an example of interhemispheric crosstalk. *Neuroreport*. 2000;11(12):2803–2809. doi:10.1097/00001756-200008210-00039
27. Peer M, Nitzan M, Bick AS, Levin N, Arzy S. Evidence for functional networks within the Human Brain's White Matter. *J Neurosci*. 2017;37(27):6394–6407. doi:10.1523/JNEUROSCI.3872-16.2017
28. Zou QH, Zhu CZ, Yang Y, et al. An improved approach to detection of amplitude of low-frequency fluctuation (ALFF) for resting-state fMRI: fractional ALFF. *J Neurosci Methods*. 2008;172(1):137–141. doi:10.1016/j.jneumeth.2008.04.012
29. Jiang F, Yu C, Zuo MJ, et al. Frequency-dependent neural activity in primary angle-closure glaucoma. *Neuropsychiatr Dis Treat*. 2019;15:271–282. doi:10.2147/NDT.S187367
30. Huang X, Zhong YL, Zeng XJ, et al. Disturbed spontaneous brain activity pattern in patients with primary angle-closure glaucoma using amplitude of low-frequency fluctuation: a fMRI study. *Neuropsychiatr Dis Treat*. 2015;11:1877–1883. doi:10.2147/NDT.S87596
31. Li T, Liu Z, Li J, et al. Altered amplitude of low-frequency fluctuation in primary open-angle glaucoma: a resting-state FMRI study. *Invest Ophthalmol Vis Sci*. 2014;56(1):322–329. doi:10.1167/iovs.14-14974
32. Martucci A, Di Giuliano F, Minosse S, Pocobelli G, Nucci C, Garaci F. MRI and clinical biomarkers overlap between glaucoma and Alzheimer's disease. *Int J Mol Sci*. 2023;24(19):14932. doi:10.3390/ijms241914932
33. Mancino R, Martucci A, Cesareo M, et al. Glaucoma and Alzheimer Disease: one age-related neurodegenerative disease of the brain. *Curr Neuropharmacol*. 2018;16(7):971–977. doi:10.2174/1570159X16666171206144045
34. Diaz-Torres S, He W, Thorp J, et al. Disentangling the genetic overlap and causal relationships between primary open-angle glaucoma, brain morphology and four major neurodegenerative disorders. *EBioMedicine*. 2023;92:104615. doi:10.1016/j.ebiom.2023.104615
35. Hayashi T, Shimazawa M, Watabe H, et al. Kinetics of neurodegeneration based on a risk-related biomarker in animal model of glaucoma. *Mol Neurodegener*. 2013;8(1):4. doi:10.1186/1750-1326-8-4
36. Yan Y, Wu Y, Xiao G, et al. White matter changes as an independent predictor of Alzheimer's disease. *J Alzheimers Dis*. 2023;93(4):1443–1455. doi:10.3233/JAD-221037
37. Yang C, Zhang W, Yao L, et al. Functional alterations of white matter in chronic never-treated and treated schizophrenia patients. *J Magn Reson Imaging*. 2020;52(3):752–763. doi:10.1002/jmri.27028
38. Zhou Y, Wang Z, Zuo XN, et al. Hyper-coupling between working memory task-evoked activations and amplitude of spontaneous fluctuations in first-episode schizophrenia. *Schizophr Res*. 2014;159(1):80–89. doi:10.1016/j.schres.2014.07.023
39. Long D, Wang J, Xuan M, et al. Automatic classification of early Parkinson's disease with multi-modal MR imaging. *PLoS One*. 2012;7(11):e47714. doi:10.1371/journal.pone.0047714
40. Choi RY, Coyner AS, Kalpathy-Cramer J, Chiang MF, Campbell JP. Introduction to machine learning, neural networks, and deep learning. *Transl Vis Sci Technol*. 2020;9(2):14. doi:10.1167/tvst.9.2.14
41. Georgevici AI, Terblanche M. Neural networks and deep learning: a brief introduction. *Intensive Care Med*. 2019;45(5):712–714. doi:10.1007/s00134-019-05537-w
42. Pereira F, Mitchell T, Botvinick M. Machine learning classifiers and fMRI: a tutorial overview. *Neuroimage*. 2009;45(1 Suppl):S199–S209.

43. Orrù G, Pettersson-Yeo W, Marquand AF, Sartori G, Mechelli A. Using Support Vector Machine to identify imaging biomarkers of neurological and psychiatric disease: a critical review. *Neurosci Biobehav Rev*. 2012;36(4):1140–1152. doi:10.1016/j.neubiorev.2012.01.004
44. Fu Q, Liu H, Zhong YL. The predictive values of changes in local and remote brain functional connectivity in primary angle-closure glaucoma patients according to support vector machine analysis. *Front Hum Neurosci*. 2022;16:910669. doi:10.3389/fnhum.2022.910669
45. Li DJ, Huang BL, Peng Y, Liang LY, Liu H. Altered dynamic functional connectivity in the primary visual cortex in patients with primary angle-closure glaucoma. *Front Neurosci*. 2023;17:1131247. doi:10.3389/fnins.2023.1131247
46. Wen Z, Wan X, Qi CX, Huang X. Local-to-remote brain functional connectivity in patients with thyroid-associated ophthalmopathy and assessment of its predictive value using machine learning. *Int J Gen Med*. 2022;15:4273–4283. doi:10.2147/IJGM.S353649
47. Tong Y, Huang X, Qi CX, Shen Y. Altered functional connectivity of the primary visual cortex in patients with iridocyclitis and assessment of its predictive value using machine learning. *Front Immunol*. 2021;12:660554. doi:10.3389/fimmu.2021.660554
48. Chen J, Jin H, Zhong YL, Huang X. Abnormal low-frequency oscillations reflect abnormal eye movement and stereovision in patients with comitant exotropia. *Front Hum Neurosci*. 2021;15:754234. doi:10.3389/fnhum.2021.754234
49. Schrouff J, Rosa MJ, Rondina JM, et al. PRoNTo: pattern recognition for neuroimaging toolbox. *Neuroinformatics*. 2013;11(3):319–337. doi:10.1007/s12021-013-9178-1
50. Hua K, Zhang J, Wakana S, et al. Tract probability maps in stereotaxic spaces: analyses of white matter anatomy and tract-specific quantification. *Neuroimage*. 2008;39(1):336–347. doi:10.1016/j.neuroimage.2007.07.053
51. Wakana S, Caprihan A, Panzenboeck MM, et al. Reproducibility of quantitative tractography methods applied to cerebral white matter. *Neuroimage*. 2007;36(3):630–644. doi:10.1016/j.neuroimage.2007.02.049
52. Zarkali A, McColgan P, Leyland LA, Lees AJ, Rees G, Weil RS. Fiber-specific white matter reductions in Parkinson hallucinations and visual dysfunction. *Neurology*. 2020;94(14):e1525–e1538. doi:10.1212/WNL.0000000000009014
53. Bubb EJ, Metzler-Baddeley C, Aggleton JP. The cingulum bundle: anatomy, function, and dysfunction. *Neurosci Biobehav Rev*. 2018;92:104–127. doi:10.1016/j.neubiorev.2018.05.008
54. Yin B, Li DD, Huang H, et al. Longitudinal changes in diffusion tensor imaging following mild traumatic brain injury and correlation with outcome. *Front Neural Circuits*. 2019;13:28. doi:10.3389/fncir.2019.00028
55. Sincoff EH, Tan Y, Abdulrauf SI. White matter fiber dissection of the optic radiations of the temporal lobe and implications for surgical approaches to the temporal horn. *J Neurosurg*. 2004;101(5):739–746. doi:10.3171/jns.2004.101.5.0739
56. Martínez-Heras E, Varriano F, Prčkovska V, et al. Improved framework for tractography reconstruction of the optic radiation. *PLoS One*. 2015;10(9):e0137064. doi:10.1371/journal.pone.0137064
57. Aralasmak A, Ulmer JL, Kocak M, Salvan CV, Hillis AE, Yousem DM. Association, commissural, and projection pathways and their functional deficit reported in literature. *J Comput Assist Tomogr*. 2006;30(5):695–715. doi:10.1097/01.rct.0000226397.43235.8b
58. Wang R, Tang Z, Sun X, et al. White matter abnormalities and correlation with severity in normal tension glaucoma: a whole brain atlas-based diffusion tensor study. *Invest Ophthalmol Vis Sci*. 2018;59(3):1313–1322. doi:10.1167/iovs.17-23597
59. Zikou AK, Kitsos G, Tzarouchi LC, Astrakas L, Alexiou GA, Argyropoulou MI. Voxel-based morphometry and diffusion tensor imaging of the optic pathway in primary open-angle glaucoma: a preliminary study. *AJNR Am J Neuroradiol*. 2012;33(1):128–134. doi:10.3174/ajnr.A2714
60. Giorgio A, Zhang J, Costantino F, De Stefano N, Frezzotti P. Diffuse brain damage in normal tension glaucoma. *Hum Brain Mapp*. 2018;39(1):532–541. doi:10.1002/hbm.23862
61. Scheck SM, Boyd RN, Rose SE. New insights into the pathology of white matter tracts in cerebral palsy from diffusion magnetic resonance imaging: a systematic review. *Dev Med Child Neurol*. 2012;54(8):684–696. doi:10.1111/j.1469-8749.2012.04332.x
62. Peltier J, Roussel M, Gerard Y, et al. Functional consequences of a section of the anterior part of the body of the corpus callosum: evidence from an interhemispheric transcallosal approach. *J Neurol*. 2012;259(9):1860–1867. doi:10.1007/s00415-012-6421-x
63. Caillé S, Sauerwein HC, Schiavetto A, Villemure JG, Lassonde M. Sensory and motor interhemispheric integration after section of different portions of the anterior corpus callosum in nonepileptic patients. *Neurosurgery*. 2005;57(1):50–9; discussion 50–9. doi:10.1227/01.NEU.0000163089.31657.08
64. Molko N, Cohen L, Mangin JF, et al. Visualizing the neural bases of a disconnection syndrome with diffusion tensor imaging. *J Cogn Neurosci*. 2002;14(4):629–636. doi:10.1162/08989290260045864
65. Epelbaum S, Pinel P, Gaillard R, et al. Pure alexia as a disconnection syndrome: new diffusion imaging evidence for an old concept. *Cortex*. 2008;44(8):962–974. doi:10.1016/j.cortex.2008.05.003
66. Li S, Sun X, Bai YM, et al. Infarction of the corpus callosum: a retrospective clinical investigation. *PLoS One*. 2015;10(3):e0120409. doi:10.1371/journal.pone.0120409
67. Uchino A, Takase Y, Nomiyama K, Egashira R, Kudo S. Acquired lesions of the corpus callosum: MR imaging. *Eur Radiol*. 2006;16(4):905–914. doi:10.1007/s00330-005-0037-9
68. Porcu M, Cocco L, Marrosu F, et al. Impact of corpus callosum integrity on functional interhemispheric connectivity and cognition in healthy subjects. *Brain Imaging Behav*. 2023;18(1):141–158. doi:10.1007/s11682-023-00814-1
69. Tusa RJ, Ungerleider LG. The inferior longitudinal fasciculus: a reexamination in humans and monkeys. *Ann Neurol*. 1985;18(5):583–591. doi:10.1002/ana.410180512
70. Chaplin TA, Rosa M, Lui LL. Auditory and visual motion processing and integration in the primate cerebral cortex. *Front Neural Circuits*. 2018;12:93. doi:10.3389/fncir.2018.00093